AFRL-RH-WP-TR-2018-0111

FIELD SAMPLING TARGETING MULTI-WALL CARBON NANOTUBE EXPOSURE DURING DESTRUCTIVE TESTING OF COMPOSITE MATERIALS

Ariel Parker
Richard Salisbury

Henry M. Jackson Foundation
For the Advancement of Military Medicine

Saber Hussain

711 HPW/RHXJ

DECEMBER 2018
Final Report

AIR FORCE RESEARCH LABORATORY
711TH HUMAN PERFORMANCE WING,
AIRMAN SYSTEMS DIRECTORATE,
WRIGHT-PATTERSON AIR FORCE BASE, OH 45433
AIR FORCE MATERIEL COMMAND
UNITED STATES AIR FORCE

NOTICE AND SIGNATURE PAGE

Using Government drawings, specifications, or other data included in this document for any purpose other than Government procurement does not in any way obligate the U.S. Government. The fact that the Government formulated or supplied the drawings, specifications, or other data does not license the holder or any other person or corporation; or convey any rights or permission to manufacture, use, or sell any patented invention that may relate to them.

Qualified requestors may obtain copies of this report from the Defense Technical Information Center (DTIC), (http://www.dtic.mil).

The experiments reported were conducted according to the "Guide for the Care and Use of Laboratory Animals," Institute of Laboratory Animal Resources, National Research Council.

AFRL-RH-WP-TR-2018-0111 HAS BEEN REVIEWED AND IS APPROVED FOR PUBLICATION IN ACCORDANCE WITH ASSIGNED DISTRIBUTION STATEMENT.

HUSSAIN.SABER.M.1283223406 Digitally signed by HUSSAIN.SABER.M.1283223406 Date: 2019.06.14 13:01:23 -04'00'

SABER M. HUSSAIN, WUM
Molecular Mechanisms Branch
Airman Systems Directorate
711th Human Performance Wing
Air Force Research Laboratory

SIMPSON.RICHARD.D.1091443429 Digitally signed by SIMPSON.RICHARD.D.1091443429 Date: 2019.06.20 16:43:00 -04'00'

RICHARD D. SIMPSON, DR-IV, DAF
Chief, Human-Centered ISR Division
Airman Systems Directorate
711th Human Performance Wing
Air Force Research Laboratory

This report is published in the interest of scientific and technical information exchange and its publication does not constitute the Government's approval or disapproval of its ideas or findings.

REPORT DOCUMENTATION PAGE

Form Approved
OMB No. 0704-0188

1. REPORT DATE *(DD-MM-YY)*	2. REPORT TYPE	3. DATES COVERED *(From - To)*
17-12-2018	Final	May 2018 – December 2018

4. TITLE AND SUBTITLE
Field Sampling Targeting Multi-Wall Carbon Nanotube Exposure During Destructive Testing of Composite Materials

5a. CONTRACT NUMBER
In-House

5b. GRANT NUMBER

5c. PROGRAM ELEMENT NUMBER
P0NQ

6. AUTHOR(S)
Ariel Parker[1], Richard Salisbury[1], Saber Hussain[2]

5d. PROJECT NUMBER

5e. TASK NUMBER

5f. WORK UNIT NUMBER
H0AQ (Historic: 7184B004)

7. PERFORMING ORGANIZATION NAME(S) AND ADDRESS(ES)
[1]Henry M. Jackson Foundation
6720-A Rockledge Drive Suite 100 Bethesda, MD 20817

8. PERFORMING ORGANIZATION REPORT NUMBER

9. SPONSORING/MONITORING AGENCY NAME(S) AND ADDRESS(ES)
[2]Air Force Materiel Command
Air Force Research Laboratory
711th Human Performance Wing
Airman Systems Directorate
Human-Centered ISR Division
Molecular Mechanisms Branch
Wright-Patterson Air Force Base, OH 45433

10. SPONSORING/MONITORING AGENCY ACRONYM(S)
711 HPW/RHXJ

11. SPONSORING/MONITORING AGENCY REPORT NUMBER(S)
AFRL-RH-WP-TR-2018-0111

12. DISTRIBUTION/AVAILABILITY STATEMENT
Distribution A: Approved for Public Release.

13. SUPPLEMENTARY NOTES
Report contains color. 88ABW-2019-2333, cleared on 13 May 2018

14. ABSTRACT

In this report, destructive processes evaluating tensile and compressive strength of materials reinforced with multi-wall carbon nanotubes (MWCNT) were sampled to investigate emission of aerosolized particulate matter (PM) targeting presence of MWCNT fragments. Generally, there was not a high increase in particulate generated by most of these processes, based on data from particle counters measuring particulate 1 micron and below in diameter. No particulate resembling representative native MWCNT was found via electron microscopy. For the slower compressive and tensile tests, increases in fine particulate (here $\leq$1 micrometer (μm)) were observed for sampling events, contrasting much lower release of ultrafine ($\leq$ 100 nanometers (nm)) particulate, although overall particle emission was low. However, the most significant process in this case, high-speed compression, showed the highest increase in both overall particulate and ultrafine particulate. Electron microscopy did not show definitive MWCNTs or MWCNT fragments, but carbonaceous "flakes" were found for all three processes sampled. Numerous small particles and small non-carbonaceous fibers were found for the final process, high-speed compression. Of the destructive processes sampled, the high-speed compression test was the most significant; however, this test also occurs several feet away from the user, and particle counts approach background counts minutes post-impact.

15. SUBJECT TERMS
Multi-wall carbon nanotubes, air sampling, mechanical testing, aerosolized particulate, particle counts, Transmission Electron Microscopy

16. SECURITY CLASSIFICATION OF:			17. LIMITATION OF ABSTRACT:	18. NUMBER OF PAGES	19a. NAME OF RESPONSIBLE PERSON (Monitor)
a. REPORT	b. ABSTRACT	c. THIS PAGE			Saber Hussain
Unclassified	Unclassified	Unclassified	SAR	29	19b. TELEPHONE NUMBER *(Include Area Code)* N/A

TABLE OF CONTENTS

Section **Page**

LIST OF FIGURES ii
LIST OF TABLES ii
ACKNOWLEDGEMENTS iii
1.0 SUMMARY 1
2.0 INTRODUCTION 2
3.0 METHOD 4
3.1 Sampling 4
3.2 Electron Microscopy 4
4.0 RESULTS AND DISCUSSION 5
4.1 Particle Count & Size Analysis 5
4.2 Electron Microscopy 10
4.2.1. SEM 10
4.2.2. S/TEM 13
5.0 CONCLUSION AND FUTURE WORK 20
6.0 REFERENCES 21
LIST OF ACRONYMS 23

LIST OF FIGURES

Figure **Page**

Figure 1. Particle Counts Measured by the Nanoscan and CPC 5
Figure 2. Nanoscan Average Particle Size Distribution for Slow Compression Test 6
Figure 3. Nanoscan Average Particle Size Distribution for Tensile Test 7
Figure 4. Nanoscan Average Particle Size Distribution for High-Speed Compression Test 8
Figure 5. Sonicated, Drop Cast Solution of Reference MWCNT, SEM 11
Figure 6. Particulate From Slow Compression Test, SEM 12
Figure 7. Particulate From Tensile Test, SEM 12
Figure 8. Particulate from High-Speed Compression Test, SEM 13
Figure 9. Sonicated, Drop Cast Solution of Reference MWCNT, TEM 14
Figure 10. Sonicated, Drop Cast Solution of Reference MWCNT with EDS, TEM 14
Figure 11. Particulate from High-Speed Compression Test, TEM 15
Figure 12. High-Speed Compression Test-Magnesium-Based Fibrous Particulate, TEM 16
Figure 13. High-Speed Compression Test-Carbonaceous Fibrous Particulate, TEM 17
Figure 14. Rod-like Particulate from High-Speed Compression Test, TEM 18

LIST OF TABLES

Table **Page**

Table 1. Average Median Diameters for Each Event Associated with Each Process 9
Table 2. Quantitative EDS for Figure 7C 13
Table 3. Quantitative EDS for Figure 10 15
Table 4. Quantitative EDS for Figure 13 17
Table 5. Quantitative EDS for Figure 14. 18

ACKNOWLEDGEMENTS

We wish to thank the Materials Characterization Facility Staff (RX) for their training and invaluable assistance.

1.0 SUMMARY

In this report, destructive processes evaluating tensile and compressive strength of materials reinforced with multi-wall carbon nanotubes (MWCNT) were sampled to investigate emission of aerosolized particulate matter (PM) targeting presence of MWCNT fragments. Generally, there was not a high increase in particulate generated by most of these processes, based on data from particle counters measuring particulate 1 micron and below in diameter. No particulate resembling representative native MWCNT was found via electron microscopy. For the slower compressive and tensile tests, increases in fine particulate (here $\leq$1 micrometer (µm)) were observed for sampling events, contrasting much lower release of ultrafine ($\leq$ 100 nanometers (nm)) particulate, although overall particle emission was low. However, the most significant process in this case, high-speed compression, showed the highest increase in both overall particulate and ultrafine particulate. Electron microscopy did not show definitive MWCNTs or MWCNT fragments, but carbonaceous "flakes" were found for all three processes sampled. Numerous small particles and small non-carbonaceous fibers were found for the final process, high-speed compression. Of the destructive processes sampled, the high-speed compression test was the most significant; however, this test also occurs several feet away from the user, and particle counts approach background counts minutes post-impact. For future studies concerned with increased or more frequent use of this analysis, operational direct-reading aerosol instruments measure particulate above 1 µm may be more informative for bundles of MWCNT rather than potential fragments; additionally, an alternate sampling method is National Institute of Occupational Safety and Health (NIOSH) Method 5040 used to detect total carbon comprised of organic and elemental carbon; total carbon can be used as an indicator of exposure.

2.0 INTRODUCTION

Since their discovery in 1991, single-wall and multi-wall carbon nanotubes (SWCNTs, MWCNTs) have proven innovative and versatile materials. Carbon nanotubes (CNTs) are nanoparticles (defined as having at least one dimension $\leq$100 nm), with diameters ranging from 1-20 nm and lengths in the micron range. Depending on the type of CNT and method of synthesis (predominantly electrical arc discharge, laser ablation ad chemical vapor deposition processes [1]), CNTs must be purified to remove residual amorphous carbon or metallic nanoparticle catalysts. MWCNTs generally have less residual metallic contamination than SWCNTs. Additionally, a key difference between SWCNTs and MWCNTs is that MWCNTs, typically more heterogeneous than SWCNTs, have weaker van der Waals forces and thus are found as single tubes or small bundles [1].

Both types of CNTs have been used in various applications due to their unique mechanical, thermal, and electrical properties [2]. Mechanically, CNTs are attractive because they possess high tensile strength (even exceeding the typical tensile strengths of high-strength steels by an order of magnitude [3, 4]) initially predicted to be 100 times stronger than steel at only $1/6^{th}$ the weight [5]. CNTs have been widely researched for reinforcing lightweight, but mechanically weak epoxy-based composites tailored for aerospace and automobile structural materials [6, 7], capable of increasing mechanical stiffness in some composites by almost 20% at only 3 wt. % addition [8].

The morphological properties, different synthesis methods, and diverse applications lead to potential CNT occupational exposure for each stage of the material's life cycle—synthesis, storage and transportation, product testing, manufacture, usage, and/or disposal. The primary exposure routes in the occupational setting are anticipated to be inhalation and dermal contact, and even secondary ingestion [9]. MWCNTs have been found among fine particulate matter aggregates in combustion streams [1], but also could be present during CNT-containing composited during machining, drilling, or wear and tear [9]. A wide variety of processes can produce airborne CNTs, so any given process potentially causing emission must be carefully examined to determine the exposure characteristics and resulting risk.

In the literature, several studies at various manufacturing sites have evaluated respiratory exposure to CNTs. These studies utilized methodologies, such as aerosol direct-reading instruments for particle number and airborne mass concentration; microscopy for PM observation; and in some cases aetholometers or organic carbon-elemental carbon discrimination to further confirm the presence of CNTs in workplaces during various workplaces and processes: chemical vapor deposition (CVD) growth [10], CNT composite fabrication and machining [11], a CNT research facility [12], CNT manufacturing plants [13], a controlled aerosol exposure and a field study of handling unrefined SWCNTs [14] . While CNTs are nanoparticulate, they are also fibrous and have been analyzed and considered to induce pathology similar to other fibrous occupational hazards, such as, asbestos and synthetic vitreous fibers [9]. Adverse respiratory health effects associated with chronic exposure to these asbestos fibers include but are not limited to lung cancer (mesothelioma), interstitial fibrosis, restricted pulmonary function, and dyspnea, according to the NIOSH Pocket Guide to asbestos.

If any airborne CNTs are not aggregated or tangled into clumps but are aerosolized such that individual CNTs or long bundles of CNTs are inhaled, they will deposit via interception within the airways like typical fibers rather than mechanisms associated with spherical particles. Regardless of fiber length, sufficiently small fiber diameters translate to aerodynamic diameters well within the diffusion regime for size-dependent particle transport, meaning sufficiently thin fibers can diffuse into the alveolar regions of the lung, just like spherical nanoparticles with the same aerodynamic diameter [15]. Thus, sufficiently long, thin, and lightweight fibers (or CNTs) can penetrate the distal/unciliated lung if their longitudinal axis is parallel to the airway stream. Human macrophages in the alveolar region of the lungs are ~15 μm, so CNTs significantly exceeding that length (lengths such as 10-20 millimeters (mm)) are more difficult to phagocytose than shorter CNTs or fragments of long CNTs, resulting in CNT build-up in the deep lung [15]. Furthermore, aside from slower clearance, long fibers have been found to induce higher pro-inflammatory effects than short fibers outside of the respiratory tract [15].

Additionally, there is an abundance of *in vivo* and *in vitro* toxicological pulmonary data from exposures to different types of CNTs. *In vitro*, pro-inflammatory responses [16], reactive oxygen species and oxidative stress [17], and phagocytosis inhibition have been observed [16, 18]. *In vivo*, inhaled CNTs exhibited most deposition in the lungs [19]. Toxicity is also concentration dependent, as a high dose in an inhalation *in vivo* study did show penetration of MWCNTs to the sub pleura, but not at a low dose [20]; in a similar study in 2010 by Porter et al, longer MWCNTs aspirated by mice (10-80 micrograms (μg)) were also found in the pleura,—which is where toxic fibers, such as asbestos induce mesothelioma [9]. The observed minimal clearance agrees with the expectation of general CNTs, graphitic materials, to be bio-persistent [15]. Other observed *in vivo* effects include granuloma formulation and inflammation [22]; and oxidative and fibrotic responses [23].

Thus, due to the known health risks described above, in this report particle count analysis and electron microscopy were used to identify potential MWCNT exposure upon destructive mechanical testing of unique materials incorporating MWCNTs.

3.0 METHOD

3.1 Sampling

Three processes were sampled: a slow compression test, a slow tensile test, and a high speed compression test. Three different sample coupons were used, one for each test. The first two tests were performed using a tens meter/universal testing machine (UTM); the first two tests with the UTM were sampled from 7 inches away. The third test was performed in another room with a custom set-up where a sample is mounted and a horizontally-oriented rod is electronically actuated for impact. Sampling occurred 4-4.5 inches away from the impact site. First, a background compression with no sample was recorded and unsuccessful compression of a sample coupon (no material failure). Finally, a successful compression of the sample.

Airborne particulate was sampled for transmission electron microscopy (TEM) analysis, onto 200 mesh nickel grids with a silicon monoxide (SiO) film (Electron Microscopy Sciences) using a Nanoaerosol Sampler (TSI, Inc.) operating at ~3.5 liters per minute (LPM) and ~-10 kilovolts (kV). A Nanoscan Scanning Mobility Particle Sizer (SMPS) 3910 (TSI, Inc.) (size range measured: 10-350 nm, over 13 bins) and Condensation Particle Counter (CPC) 3007 (TSI, Inc.) (size range measured: 10 – 1000 nm) were used to measure particle counts over time during testing. Each test was sampled for five minutes post-impact. The Nanoscan measures particle size distribution and concentration every minute, whereas the CPC logs particle counts within its size range every second.

An Optical Particle Sizer 3300 (TSI, Inc.) was also used during sampling to measure particle concentration and size classification (size range 0.3 – 10 μm), but for all processes showed negligibly low or no particle counts, which is likely due to instrument malfunction.

3.2 Electron Microscopy

Both TEM and Scanning Electron Microscopy (SEM) were used to evaluate morphology and chemical composition of air-sampled particulate using Energy-Dispersive X-Ray Spectroscopy (EDS). For SEM, the Gemini500 (Zeiss) was used for imaging and EDS was performed with Aztec One software, and an Ultimate Extreme Silicon Drift Detector (Oxford Instruments). For TEM, an FEI Telos F200X (Thermos Fisher) was used for visualization and Esprit (Bruker) software was used for EDS analysis. Prior to analysis with the TEM, the grids were sputter-coated with 2 nm of iridium to prevent charging effects by the SiO film. NIH Image was used to measure fibrous particulate dimensions.

4.0 RESULTS AND DISCUSSION

4.1 Particle Count & Size Analysis

Based on Figure 1, during tests, regardless of room, background remains below 2000 particles/cubic centimeter (cm^3). Doors opened/closed, ventilation? CPC particle counts, encompassing a larger size range, overall are higher than Nanoscan counts, but the trends are the same for both instruments for all processes where both recorded data. CPC show overall higher particle counts than SMPS, indicating highest number of particle counts are contributed by particles with diameters 0.4 $\leq$ Particle diameter (dP) $\leq$ 1 micron. However, the CPC does not classify particles by size, so although the particle counts here indicate that there are particles in the size bin 0.4-1 micron, this data alone cannot indicate what may be the median particle diameter for the size range 10 nm – 1 micron. Based on the particle count data, the only test of concern is the high-speed compression test, which also occurs the furthest away from the user.

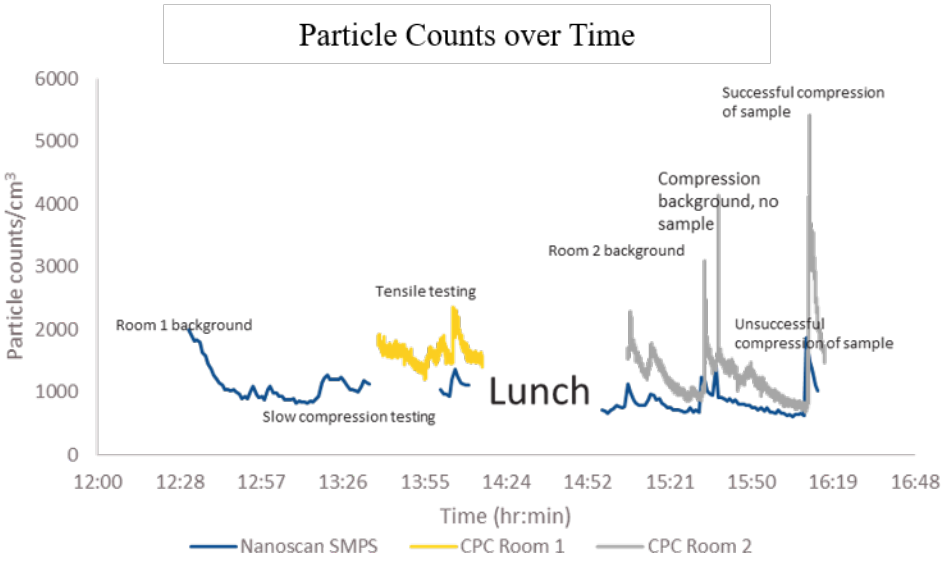

Figure 1. Particle Counts Measured by the Nanoscan and CPC

Sampling spanned all three processes. The CPC malfunctioned during the first test so no data was successfully recorded.

However, while the data from the particle counters does give a general idea of airborne particulate concentration, the counters assume spherical particles with a density of 1.2 g/cubic centimeter (ccm)--MWCNTs may aerosolize as fragmented bundles and potentially have a lower density of 1.2 g/ccm. Nonetheless, these default values help identify specific trends associated with the processes sampled. Additionally, the particle count levels detected here are well below the instruments' saturation levels (~1E6 particles/cm^3 for the Nanoscan, ~1E5 for the CPC).

Overall, as Figure 1 shows, the slow tests performed in Room One did not show high increase in particle counts compared to background regardless of particle counter used. For all tests particle counts seemed to re-stabilize to or approach background quickly. Background readings from the Nanoscan in Room One were erratic, and dropped by half before the slow compression test began (Figure 1). Background readings, once they dropped, stayed ~1000 particles/cm^3 and increased slightly up to ~1200 particles/cm^3. The slow compression test spanned 13:27-13:34 in Figure 1. During the slow compression, the counts stayed slightly above 1200 particles/cm^3 and for the five minute post-test interval there was no significant change. The CPC malfunctioned during this test, so only Nanoscan data was considered. The median diameter, according to the Nanoscan, was ~50 nm during the slow compressive test and slightly smaller for most background readings.

The slow compression test shows a difference in the Nanoscan's average particle size distribution; the compression data indicates a broader presence of particle sizes and an increase in the amount of particles greater than 100 nm or below 20 nm (Figure 2). The average median diameter does not change (Table 1), although the average distribution does. However, the difference in the peak diameter with the highest size fraction indicated in Figure 2 is not large enough to greatly impact deposition characteristics of those particulates. This may also be in part, because the background concentrations were erratic, indicating that the concentrations of specific size bins may also be more erratic, skewing the average distribution measured over that time.

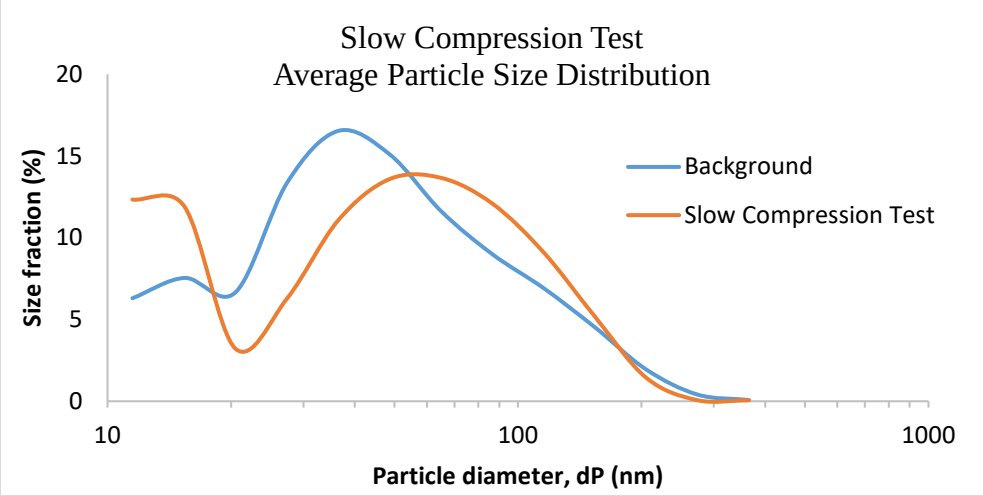

Figure 2. Nanoscan Average Particle Size Distribution for Slow Compression Test

Slight shift in median diameters for background and slow compression test average particle size distributions.

Only the duration of the tensile test was measured with the Nanoscan without more background measurements between the tensile and compression tests; the CPC measured particle counts pre-

during, and post-test (Figure 1). In this test, the dog bone-shaped coupon was pulled on either end in a vertical orientation till sample failure (i.e., breakage). According to Figure 1, the tensile load was applied at 14:07, and the sample failed at 14:10, corresponding to an increase in particle counts for both instruments. For the Nanoscan readings, there is an increase of ~300 particles/cm^3 compared to the pre-failure readings. The CPC's peak is closer to 2500 particles/cm^3, and is an increase of 1000 particles/cm^3 from the lowest reading. Nonetheless, pre- and post-test readings mostly remain close to 2000 particles/cm^3. Additionally, the average particle size distribution and average median diameters did not change between pre-sampling and the test itself (Figure 3).

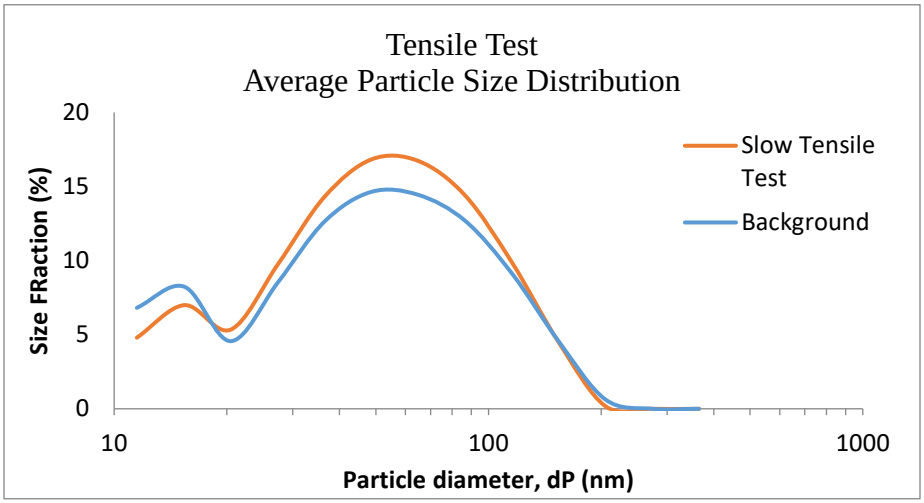

Figure 3. Nanoscan Average Particle Size Distribution for Tensile Test

No shift in median diameters for background and tensile test average particle size distributions.

Finally, the high-speed compression tests yielded the highest increase in particle concentration for both instruments. Nanoscan background readings started lower in Room Two than Room One, but was similarly erratic. Interestingly, CPC background counts prior to testing were in a similar range with peaks comparable to the tensile test. Regarding the background compression without a sample, Nanoscan readings increased from ~700 particles/cm^3 to ~1400 particles/cm^3; and for the successful compression, particle counts peaked at ~1900 particles/cm^3. However, the CPC, while showing the same trends in particle concentration over time as the SMPS, shows a significant increase upon impact from ~800 particles/cm^3 to almost 5000 particles/cm^3 during the successful compression. In the high-speed compression scenario (Figure 4), the unsuccessful compression did not produce any particles in the Nanoscan's size range, but did cause a slight increase for the CPC's larger size range.

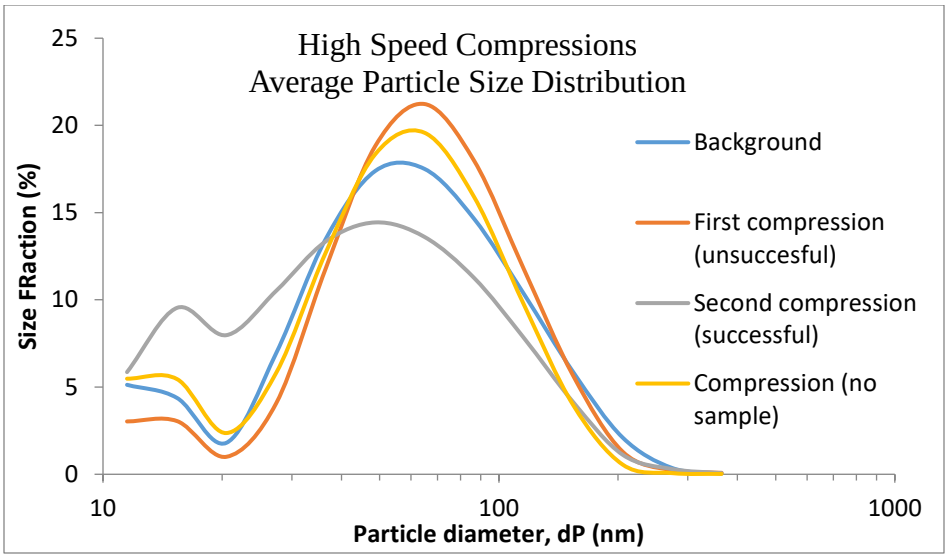

Figure 4. Nanoscan Average Particle Size Distribution for High-Speed Compression Test

Slight shift in median diameters for events and background during high-speed compression test.

The apparent differences between particle counts between the Nanoscan and CPC are most pronounced in the high-speed compression test, and likely arise due to the difference in size ranges compatible with each instrument. Furthermore, overall particle counts at the test site appear to fall back to baseline levels; although the five minute post-sampling period was not long enough to observe particle counts decreasing to baseline, the peak and subsequent downward trend, even with the unsuccessful sample compression, corresponding to the no-sample compression test indicate it would decrease in minutes. Additionally, as CNTs are lauded as having impressive mechanical strength for their size, it agrees with the data for both compression tests here suggesting that a higher impact delivering a larger amount of force would be required to cause sample failure and potential MWCNT dispersal into the air.

Although no CPC data was successfully recorded for the first slow compression test, from Figure 1, the Nanoscan data stayed in the same range for both slow tests. For the rest of the sampling, the CPC exaggerated the peaks and trends observed in the rest of the Nanoscan data, so while overall inconclusive it is likely that CPC data for this process would follow Nanoscan trends on a larger particle count scale, and be comparable to the tensile test data.

Furthermore, the change in median diameter from ~48 nm to 50-51 nm from the compression test compared to the tensile test is not large enough to greatly impact deposition characteristics of those particulates, and also indicates lack of a detectable unique aerosol (marked by distinct median diameter) produced by the sample breakage. The median diameter did change for the four events contained in the high-speed compression scenario: background, no-sample compression, unsuccessful compression of sample, and successful compression of sample (Table 1).

Table 1. Average Median Diameters for Each Event Associated with Each Process

Compression and tensile test average include five minutes post-failure sampling to account for any sample particulate remaining near the sampling site.

Event	Average Median Diameter (nm)
Background, Room 1 (Slow Compression)	48.01
Compression	48.01
Background/Pre-Test, Room 1 (Slow Tensile Test)	50.53
Tensile Test	51.61
Background, Room 2 (High-speed Compressions)	58.45
Compression (no sample)	56.60
First Compression (Unsuccessful)	64.37
Second Compression (Successful)	50.16

The lack of significant change in ultrafine particle counts generally agrees with some previous studies for airborne MWCNTs and SWCNTs, since some of these did not detect particulate increases for particles less than one micron, but in fact between two to three microns [12, 14]. These size distributions were associated with laboratory-aerosolized SWCNTs [14] and facilities performing MWCNT production and handing of unrefined materials [12]. Similarly, heightened particle concentrations (increasing an order of magnitude, 1E4 to 1E5) were often associated with manual handling of MWCNTs, furnace opening, and sonication [24].

Although microscale diameters often arise from aggregation and tangling of single CNTs, the median diameter is also process-dependent; significant nanoscale particulate exposure of CNTs has been shown to be present at facilities dedicated to synthesis and/or manufacture of CNTs during opening CVD growth chambers [24].

In a 2009 field study, dry cutting of composites yielded increases two orders of magnitude for ultrafine particulates and microscale particulates (minimum 15 particles/cm^3, maximum 2000 particles/cm^3) [11]. While the upper bound is in the same order of magnitude as the data presented here, Bello's difference from background is much more significant. However, in Bello et al's 2008 study [10] sampling at a facility producing substrate-bound CNT growth via CVD, particle counts over time and changes in particle counts were comparable to levels measured here and were not a considered a health risk to workers.

Based on the conclusions in the literature, the particle count analysis spanning 10-1000 nm for the destructive processes measured here do not indicate a health risk, especially, for the slow destruction processes. Additionally, all processes occur a few feet away from the user, and for the high-speed compression test, the largest distance away.

4.2 Electron Microscopy

4.2.1. SEM

The Gemini SEM used in this report has the capability of imaging in SEM or TEM mode, and used as a screening tool to more quickly detect micron-length particulate and to do lower-resolution EDS analysis; TEM was used for samples requiring higher-resolution EDS and/or ultrafine fragments requiring a regular TEM's superior resolution. Ultrafine fragments difficult to adequately resolve visually or to identify with lower-energy EDS available with SEM were found on the high-speed compression grid, and were examined at higher resolution in the TEM. Reference MWCNTs (outer diameter 6-13 nm, length 2.5-20 micron; Sigma Aldrich) were easily visible using Scanning Transmission Electron Microcopy (STEM) on the Gemini, so any MWCNTs could be resolved well enough for identification in the Gemini. However, these reference MWCNTs are not the same MWCNTs used in the composite material coupons destructively tested.

Other studies [12, 10, 24] found airborne CNTs resembling clumps for certain processes (e.g. sonication or opening a furnace involved in catalyst preparation) not unlike the reference MWCNT (Figure 5). However, these field studies were at CNT Production Facilities or where the raw material is synthesized, packaged, transported, etc. Thus, it would be expected that in a process involving mechanical processes of a composite containing MWCNT, smaller MWCNT fragments are possibly coated in matrix material or are embedded in larger pieces of particulate [11, 25].

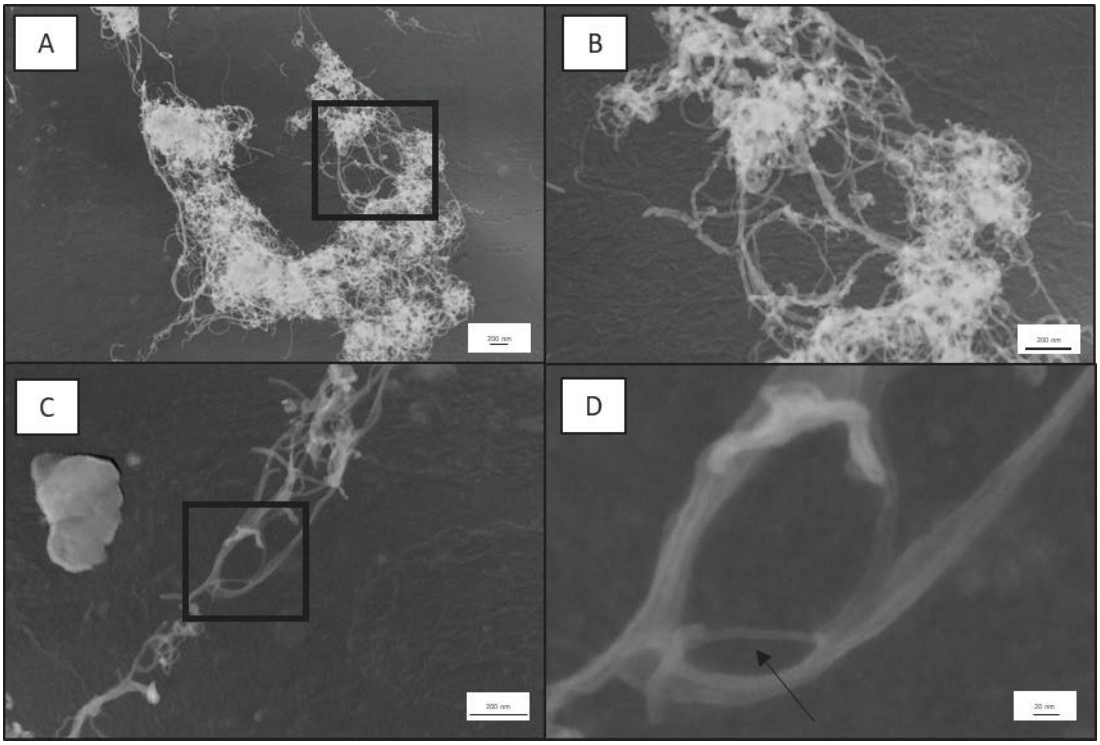

Figure 5. Sonicated, Drop Cast Solution of Reference MWCNT, SEM

A) MWCNT clump. B) Inset of (A).
C) "Ropes" of MWCNT. D) Inset of (C). Arrow indicates individual MWCNT.

Figures 6-8 are SEM images of particulate collected during destructive testing of sample coupons:

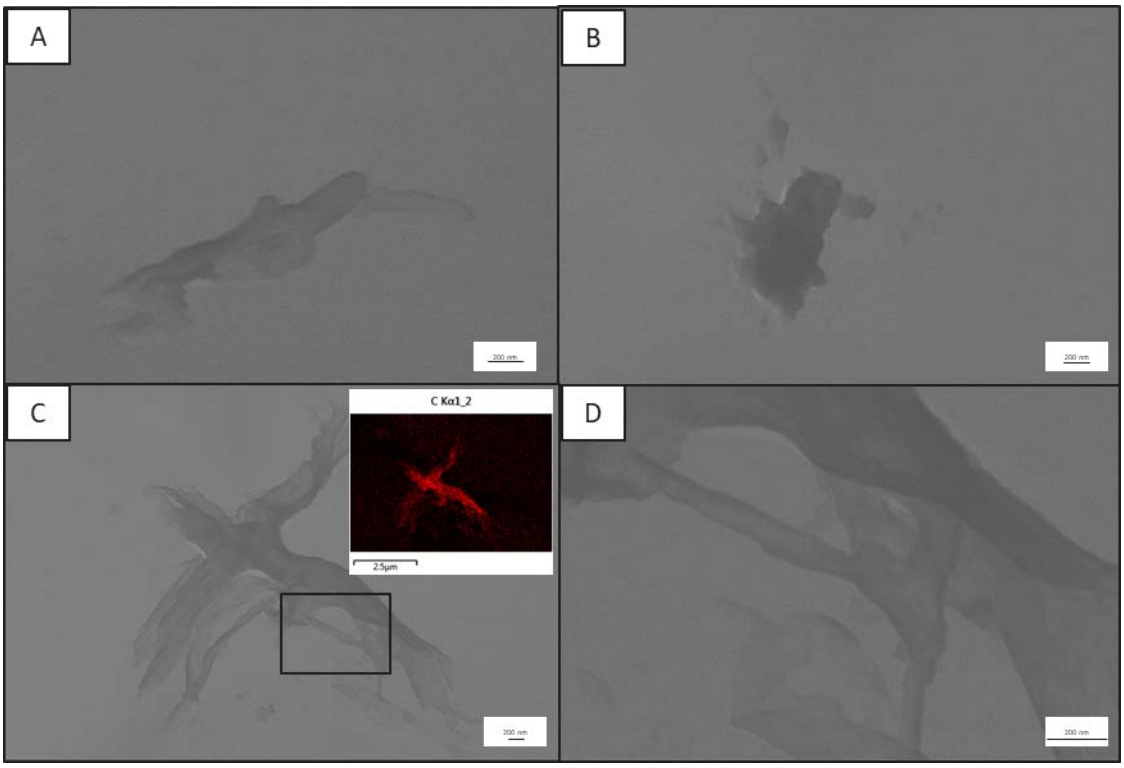

Figure 6. Particulate From Slow Compression Test, SEM

A) Flake-like particle, B) Carbonaceous clump with nitrogen signature, C) Carbonaceous flake-like bundle or particle (upper left hand corner shows carbon map via EDS), D) Inset of C).

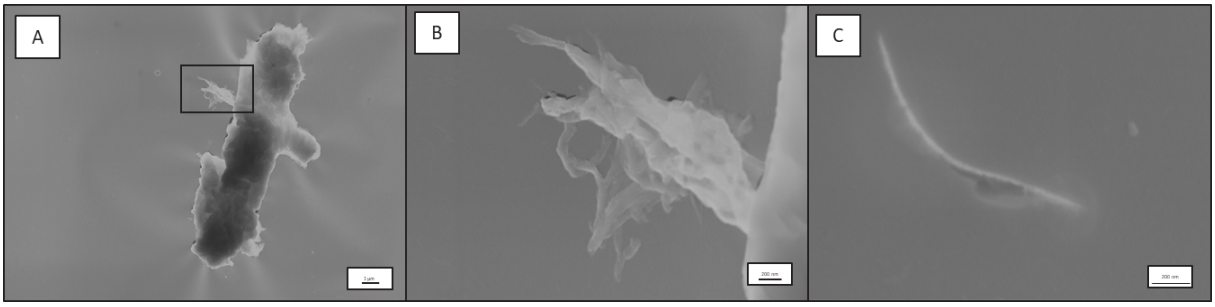

Figure 7. Particulate From Tensile Test, SEM.

A) Unidentified large particulate with flake-like morphology extending from one edge, B) Inset of (A). Carbonaceous flake-like bundle or particulate, C) Carbonaceous fibrous particulate with clump attached. Quantitative EDS indicates twice as much C in fiber than on grid background (Table 2).

Table 2. Quantitative EDS for Figure 7C

Element	Fiber (wt. %)	Background (wt. %)
C	49.09	28.42
O	31.90	38.79
Si	19.01	32.79

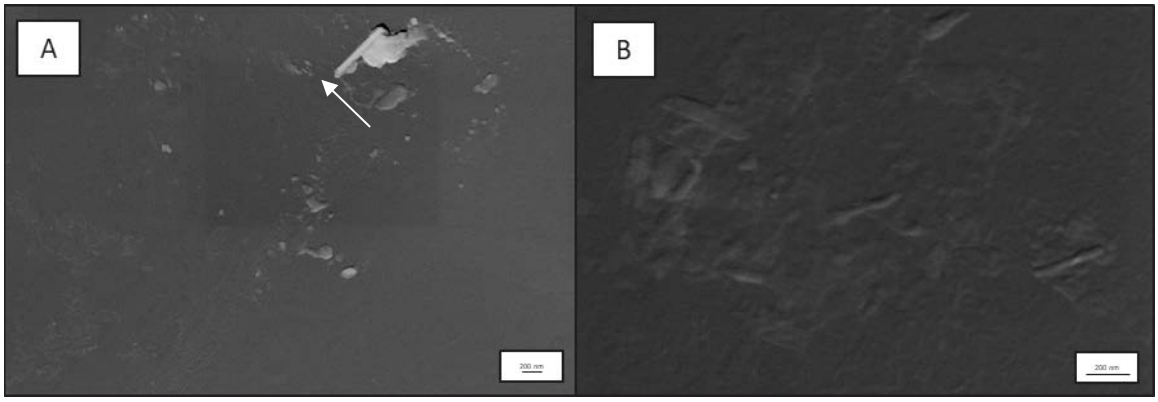

Figure 8. Particulate from High-Speed Compression Test, SEM

A) Several fine and ultrafine particulates. The clump indicated by the arrow features a rod-like particulate ~70 nm across and half a micron long, B) Possible fibrous particulate (~20 nm across). No reliable EDS data was obtained with this grid using SEM due to charging issues

Since more submicron and/or ultrafine particulate as shown above in (A) was visible on the high-speed compression sample, corroborating the Nanoscan data shown in Figure 1. Due to the failed EDS and resolution limits of the SEM in TEM or STEM mode, both the high-speed compression and stock MWCNTs were evaluated with the Telos TEM. Both the high-speed compression test grid and stock MWCNT grids were examined for morphology and elemental analysis with the higher resolution; TEM with greater EDS capabilities since this test yielded the highest particle count overall and highest ultrafine particle count increase.

4.2.2. S/TEM

With the Telos TEM, both bright field (traditional TEM imaging), and STEM, (a High-Angle Annular Dark Field (HAADF) Technique) can be performed. Both are capable of high resolution imaging, but TEM images transmit electrons through the particulate, while STEM scans in a raster pattern over the region of interest and images show a topography. Elemental mapping shown here was done in STEM mode. Below (Figure 9 and 10), bright field, dark field, and EDS images are shown for reference MWCNT.

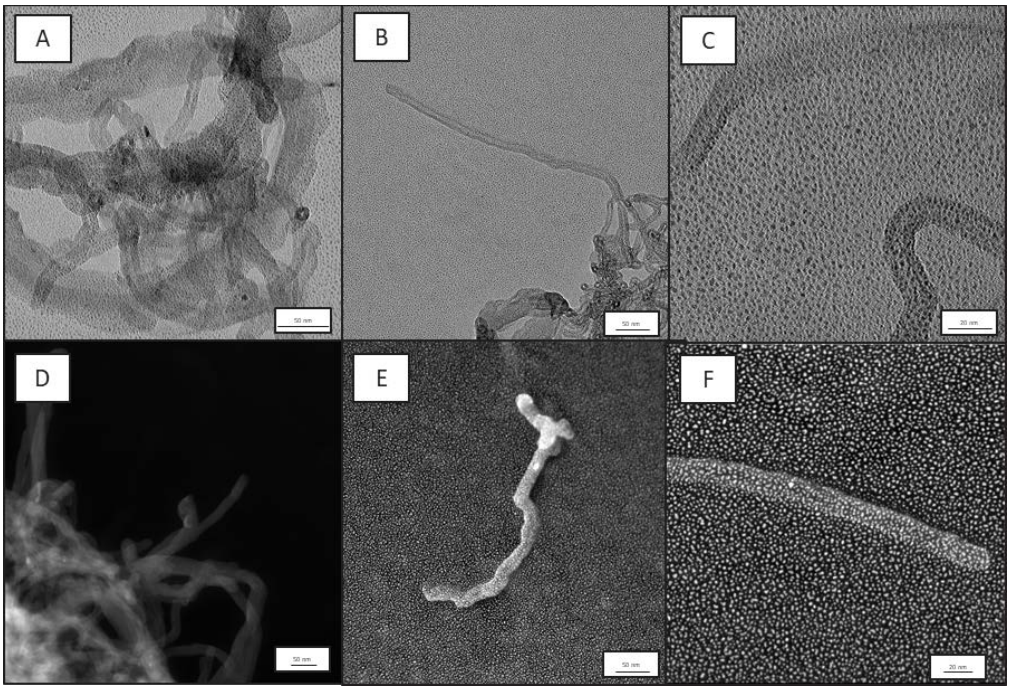

Figure 9. Sonicated, Drop Cast Solution of Reference MWCNT, TEM

A-C) Bright field images of MWCNT, D-F) STEM, HAADF images of MWCNT.

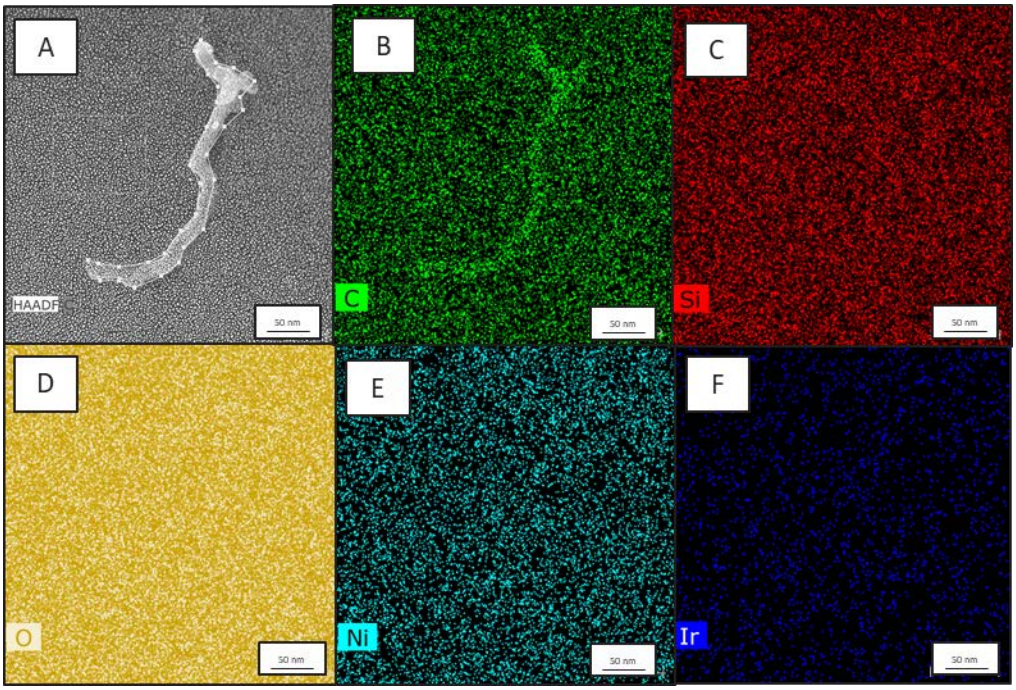

Figure 10. Sonicated, Drop Cast Solution of Reference MWCNT with EDS, TEM

A) HAADF map image of 9E, B-F) Elemental maps detected indicating slight localization of carbon overlaid with particulate.

Table 3. Quantitative EDS for Figure 10

Element	Background [wt.%]	MWCNT [wt.%]
C	17.81	24.60
Ir	9.38	10.29
Ni	12.35	12.53
O	26.49	23.24
Si	33.97	29.34

Although the carbon concentration increase is not as high as for Figure 13B, the reference MWCNT showed a signal ~7% than background.

In comparison, the following images are of particulate found on the high-speed compression sample. Like the SEM images of the other two samples, some flake-like carbonaceous material was found, particularly Figure 11 below:

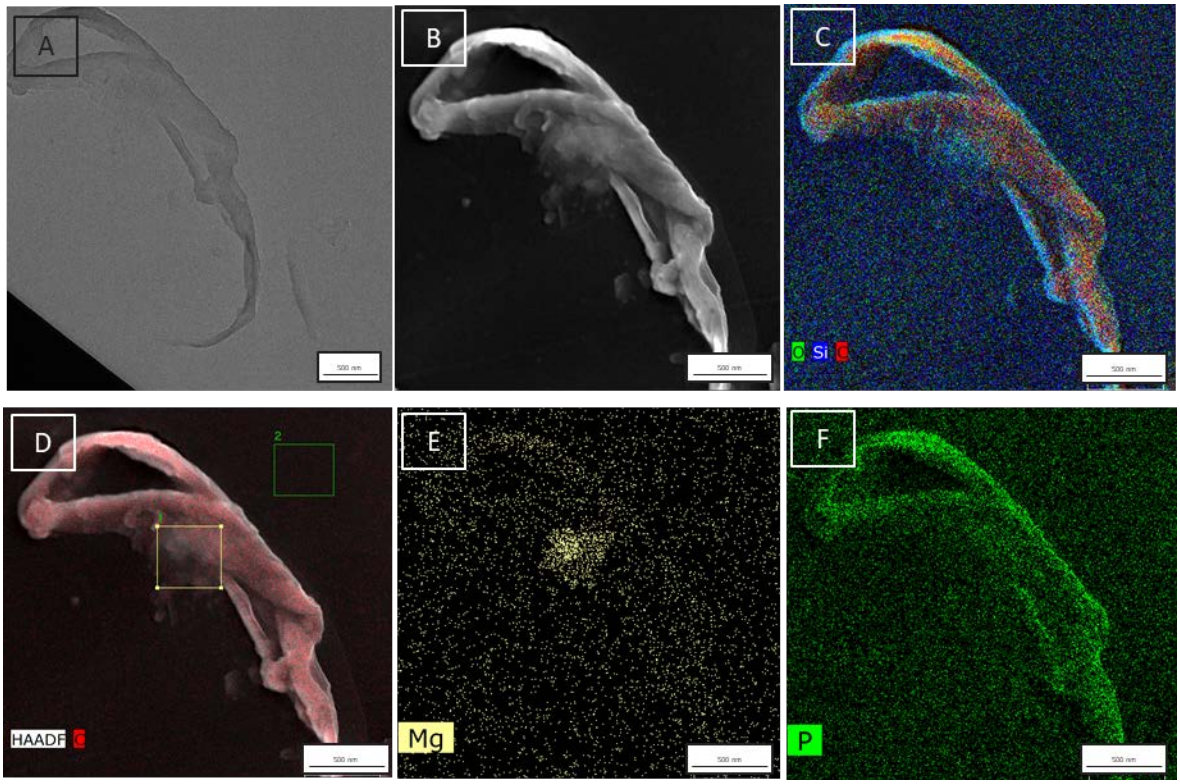

Figure 11. Particulate from High-Speed Compression Test, TEM

A) Flake-like bundle particulate in bright field, B) Flake-like bundle particulate in dark field. C) – F) Various elements detected via EDS mapped over particulate.

Magnesium fibers in Figure 12 are on the nanoscale and definitely have the potential to enter the deep lung if inhaled; however, the aspect ratio is low so these “short” fibers or rods are much more capable of being phagocytosed and cleared by macrophages, at least on a size basis. The magnesium fiber is Figure 12A is ~35 nm in diameter, ~79 nm in length; the one in F is ~8 nm in diameter, ~115 nm in length.

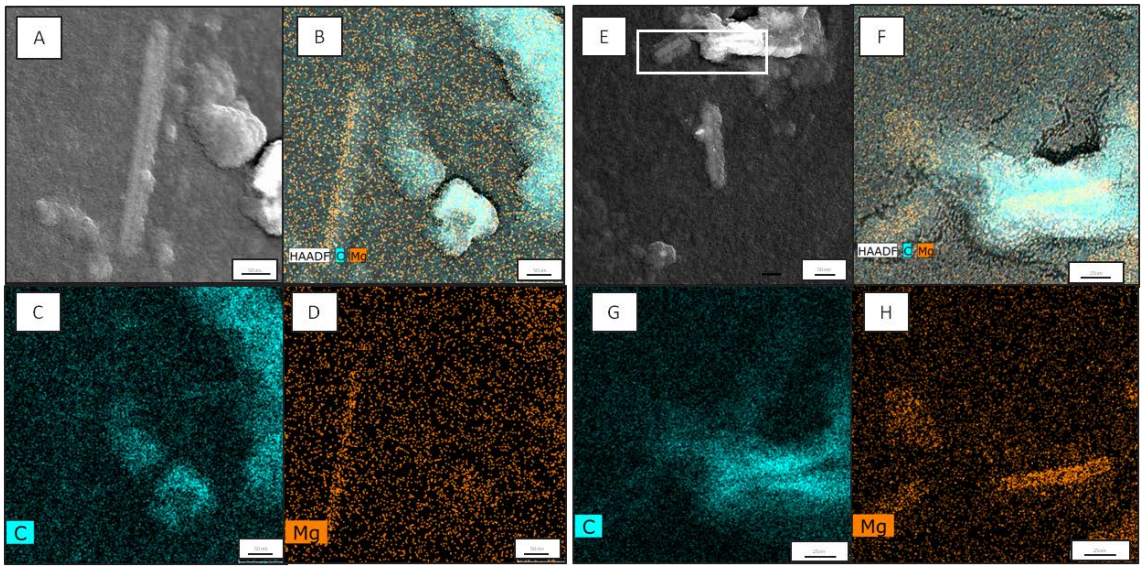

Figure 12. High-Speed Compression Test-Magnesium-Based Fibrous Particulate, TEM

Carbon and magnesium elemental maps shown, A) One magnesium “fiber.” B-D) Elemental maps of (A), E) Two “fibers,” F-H) Elemental maps of inset in (E).

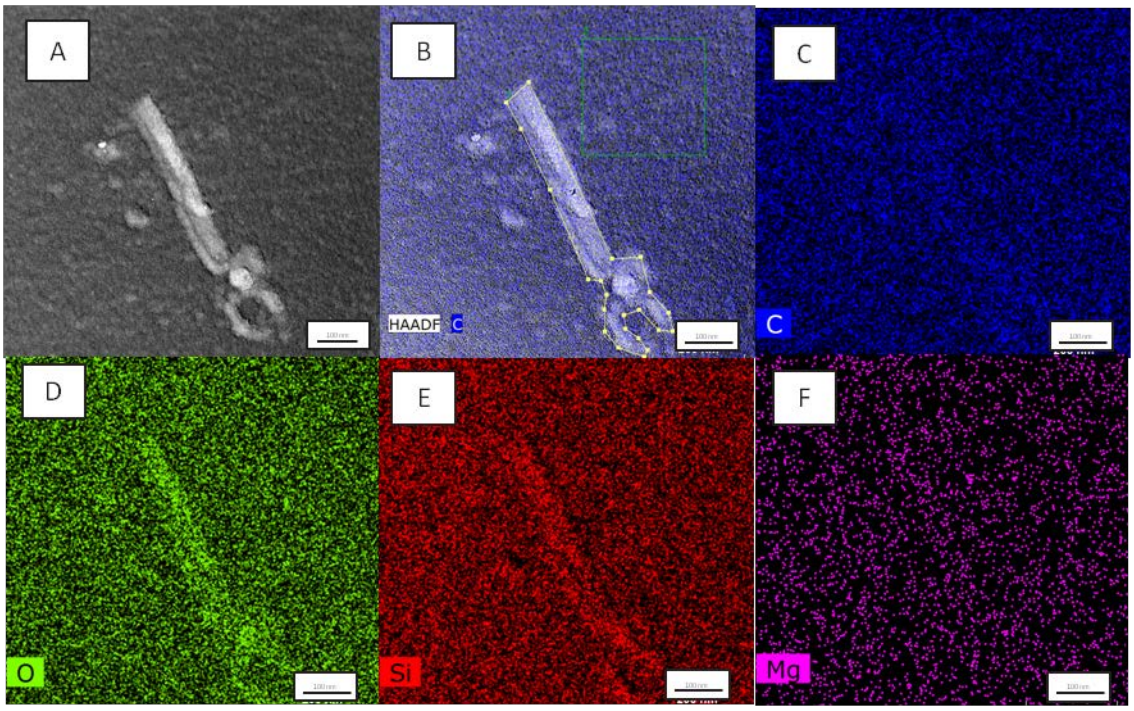

Figure 13. High-Speed Compression Test-Carbonaceous Fibrous Particulate, TEM

A) HAADF image of fibrous particulate B-F), various elemental maps, Quantitative analysis shows almost no difference between the particulate and the grid film background for C content.

Table 4. Quantitative EDS for Figure 13

Element	Particulate [wt.%]	Background [wt.%]
Al	1.06	0.00
C	6.52	6.32
Ir	9.40	10.67
Fe	0.37	0.00
Ni	23.44	27.05
O	25.90	23.99
K	0.45	0.00
Si	32.86	31.98

Figure 14 was the closest positive identification of a CNT observed in these sample grids. EDS indicates a localization of C, and quantitative analysis shows a significant difference between the tube/rod-like structure and grid film background (Table 5).

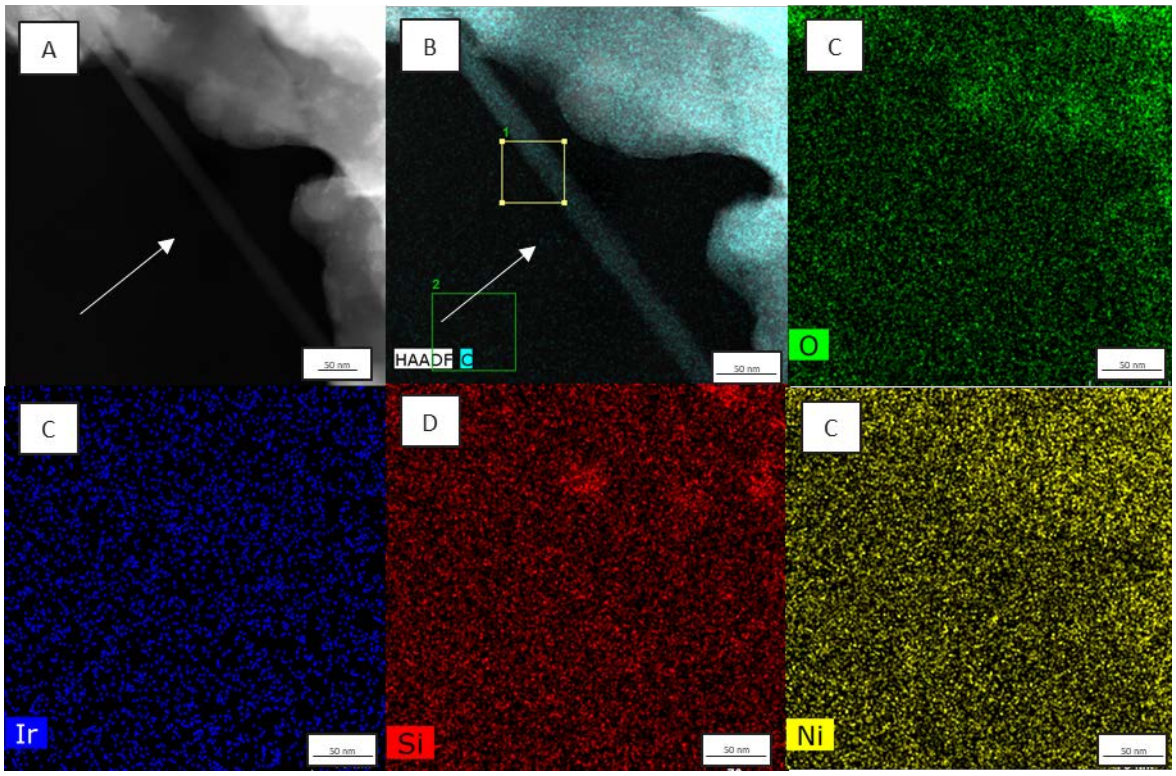

Figure 14. Rod-like Particulate from High-Speed Compression Test, TEM

A) STEM image with possible CNT, ~ 20 nm in diameter/ width, B) Elemental map of C overlaid with HAADF image showing localization of C, C-F). Various maps of background elements. Other elements corresponding to the mass in the upper-left hand corner were also identified but not shown (e.g. sodium, calcium, etc.).

Table 5. Quantitative EDS for Figure 14.

Element	**Rod [wt.%]**	**Background [wt.%]**
C	29.06	6.32
Ir	8.45	12.58
Ni	22.33	29.91
O	14.75	18.35
Si	25.42	32.85

Some of the fibrous particulate found among the high-speed compression particulate was magnesium (Figure 12). Other images not displayed here showed some of these magnesium rods or fibers embedded within larger clumps of material that tended to be carbonaceous. Barium-based fibers and particles (dP on the order of 10 nm) were also found in concentrated areas.

Figure 14B above had the most significant carbon concentration and appeared to be in the range of the correct dimensions for CNTs. However, multiple short rod-like particulates (possible MWCNT fragments), such as that in Figure 13 were imaged and analyzed via EDS, but had a carbon signal virtually identical to background (Table 3).

The quantitative EDS analysis performed for the single reference MWCNT showed a smaller increase in carbon (Figure 10) than the rod-like structure in Figure 14. It is possible that since the single MWCNT in Figure 10 is clearly on the grid's support film the carbon background is already much higher and since MWCNTs are so small, they contribute little extra carbon signal. Furthermore, in Figure 14, the rod is partially attached to a larger clump with a high localization of carbon and some signal from that clump could have been detected and counted in the analysis of the rod; also, it is difficult to definitely distinguish, but the rod maybe be slightly elevated and inclined, based on the fading intensity from the top left of Figure 14A to the bottom right. If the rod is slightly elevated, that could contribute to a lower background signal for this particular map compared to other maps presented in this report.

In the various workplaces and processes evaluated in previous studies [10-14, 24], most particulate imaged via electron microscopy resembled clumps or bundles, usually not as individual fibers. Of these previous reports, Bello et al's 2009 study analyzing CNT emission during wet and dry cutting of CNT-reinforced composites, among other processes, was most analogous to the processes sampled here; they had similar difficulty identifying CNTs in the particulate they sampled. Possible explanations proposed by Bello et al included that CNTs were clumped or encapsulated into the matrix material and so individual CNTs could not be identified; that the CNTs themselves bound together while in the composite matrix and produce larger fibers or particulates than the functioning particle counters could detect; or CNTs/CNT fragments may simply not be emitted during testing [11, 12, 13].

However, based on these suggestions, for the data in this report it seems more likely that any MWCNTs are embedded into larger particulates. Depending on how they are processed within the overall sample matrix, the MWCNTs could somehow bind or fuse together into the flake-like structures identified to have higher carbon content than grid background for all samples.

Finally, in Methner's Field Study for CNT Exposure, an additional method to supplement the particle count analysis and microscopy was achieved by adapting NIOSH Method 5040 to detect the total carbon (TC) in $\mu g/m^3$ associated with each process the team sampled [24]. NIOSH method 5040 is used to determine the total carbon content in diesel particulate matter by detecting the organic and elemental carbon; summed together, these quantities constitute total carbon. Methner et al used this method to sample and quantify CNTs presence at several sites, including one producing composite materials incorporating CNTs [24]. Their results showed decreased particle counts (in the 10-1000 nm range) and increased mass concentration compared to background measurements. Both processes exceeded the Mine Safety and Health Administration's (MSHA) recommendation for maximum TC exposure limit of 160 $\mu g/m^3$.

5.0 CONCLUSION AND FUTURE WORK

Based on the images and available data, no definitive MWCNT fragments were found and particulate in the 0.4-1 micron range and was more prevalent than particulate, smaller than 0.4 µm. The slow destructive processes did not emit large concentrations of particles in the 10-1000 nm range compared to background readings. The average median size during background and during the ~5 minute long tests did not change much in the 10-400 nm range. The high-speed compression test, however, did produce the highest amount of particulate, which seemed to mostly in the 0.4-1 micron range. Below 400 nm, for the four events encompassed in the test, there is a leftward shift of the average particle size distribution and a change in the average median diameter associated with the duration of each event. Microscale carbonaceous flake-like particulate was observed in SEM samples of both slow and fast destructive processes, but the increased amount of particles, and of smaller particles, required higher-resolution TEM and EDS for the high-speed compression sample. Several short fibers were observed, but some were not carbon-based and others did not have a carbon signal appreciably above background. In contrast, reference MWCNTs did have higher increases in carbon signal compared to background, although these reference MWCNTs are not necessarily the same as the ones applied to the sample materials here. Nonetheless, based on the particle counters, amount of samples and tests performed, testing set-up and environment, it is likely there is no actionable health hazard. Should these materials require more frequent tests and if the materials themselves require an increase in wt. % MWCNTs, similar particle count emission should be monitored through the supra micron range as well. If microscopy is the method of analysis, the MWCNTs used and a dedicated composite sample coupon should be prepared and imaged for reference so any airborne particulate can be more easily identified. For a faster turn-around time than microscopy, adapting NIOSH Method 5040 as described in Methner's Study is recommended.

6.0 REFERENCES

1. Lam, Chiu-wing, et al. "A review of carbon nanotube toxicity and assessment of potential occupational and environmental health risks." *Critical reviews in toxicology* 36.3 (2006): 189-217.

2. Montazeri, Arash, et al. "Mechanical properties of multi-walled carbon nanotube/epoxy composites." *Materials & Design* 31.9 (2010): 4202-4208.

3. Demczyk, Brian G., et al. "Direct mechanical measurement of the tensile strength and elastic modulus of multi-walled carbon nanotubes." *Materials Science and Engineering: A* 334.1-2 (2002): 173-178.

4. Bacon, Roger. "Growth, structure, and properties of graphite whiskers." *Journal of Applied Physics* 31.2 (1960): 283-290.

5. Smalley, R. E. "Nanotechnology. Prepared written statement and supplemental material of RE Smalley, Rice University, June 22, 1999." *US House of Representatives Committee on Science, Basic Research Subcommittee Hearings* (1991).

6. Frisch, Harry L., and James E. Mark. "Nanocomposites prepared by threading polymer chains through zeolites, mesoporous silica, or silica nanotubes." *Chemistry of Materials* 8.8 (1996): 1735-1738.

7. Park, Jonghyun, and Sadhan C. Jana. "Effect of plasticization of epoxy networks by organic modifier on exfoliation of nanoclay." *Macromolecules* 36.22 (2003): 8391-8397.

8. Zhou, Yuanxin, et al. "Fabrication and evaluation of carbon nano fiber filled carbon/epoxy composite." *Materials Science and Engineering: A* 426.1-2 (2006): 221-228.

9. Aschberger, Karin, et al. "Review of carbon nanotubes toxicity and exposure—Appraisal of human health risk assessment based on open literature." *Critical reviews in toxicology* 40.9 (2010): 759-790.

10. Bello, Dhimiter, et al. "Particle exposure levels during CVD growth and subsequent handling of vertically-aligned carbon nanotube films." *Carbon* 46.6 (2008): 974-977.

11. Bello, Dhimiter, et al. "Exposure to nanoscale particles and fibers during machining of hybrid advanced composites containing carbon nanotubes." *Journal of Nanoparticle Research* 11.1 (2009): 231-249.

12. Han, Jeong Hee, et al. "Monitoring multi-walled carbon nanotube exposure in carbon nanotube research facility." *Inhalation toxicology* 20.8 (2008): 741-749.

13. Lee, Ji Hyun, et al. "Exposure assessment of carbon nanotube manufacturing workplaces." *Inhalation toxicology* 22.5 (2010): 369-381.

14. Maynard, Andrew D., et al. "Exposure to carbon nanotube material: aerosol release during the handling of unrefined single-walled carbon nanotube material." *Journal of Toxicology and Environmental Health, Part A* 67.1 (2004): 87-107.

15. Donaldson, Ken, et al. "Carbon nanotubes: a review of their properties in relation to pulmonary toxicology and workplace safety." *Toxicological sciences* 92.1 (2006): 5-22.

16. Brown, D. M., et al. "An in vitro study of the potential of carbon nanotubes and nano fibres to induce inflammatory mediators and frustrated phagocytosis." *Carbon* 45.9 (2007): 1743-1756.

17. Pulskamp, Karin, Silvia Diabaté, and Harald F. Krug. "Carbon nanotubes show no sign of acute toxicity but induce intracellular reactive oxygen species in dependence on contaminants." *Toxicology letters* 168.1 (2007): 58-74.

18. Boyles, Matthew SP, et al. "Multi-walled carbon nanotube induced frustrated phagocytosis, cytotoxicity and pro-inflammatory conditions in macrophages are length dependent and greater than that of asbestos." *Toxicology in Vitro* 29.7 (2015): 1513-1528.

19. Deng, X., et al. "Translocation and fate of multi-walled carbon nanotubes in vivo." *Carbon* 45.7 (2007): 1419-1424.

20. Ryman-Rasmussen, Jessica P., et al. "Inhaled carbon nanotubes reach the sub-pleural tissue in mice." *Nature nanotechnology* 4.11 (2009): 747.

21. Porter, Dale W., et al. "Mouse pulmonary dose-and time course-responses induced by exposure to multi-walled carbon nanotubes." *Toxicology* 269.2-3 (2010): 136-147.

22. Warheit, David B., et al. "Comparative pulmonary toxicity assessment of single-wall carbon nanotubes in rats." *Toxicological sciences* 77.1 (2004): 117-125.

23. Shvedova, Anna A., et al. "Inhalation versus aspiration of single walled carbon nanotubes in C57BL/6 mice: inflammation, fibrosis, oxidative stress and mutagenesis." *American Journal of Physiology-Lung Cellular and Molecular Physiology* (2008).

24. Methner, M., et al. "Nanoparticle emission assessment technique (NEAT) for the identification and measurement of potential inhalation exposure to engineered nanomaterials—Part B: Results from 12 field studies." *Journal of occupational and environmental hygiene* 7.3 (2010): 163-176.

25. Gupta, A., et al. "Evaluating the potential for release of carbon nanotubes and subsequent occupational exposure during processing of a nanocomposite." *Nanotechnology occupational and environmental health and safety* (2006).

LIST OF ACRONYMS

cm	Centimeter
nm	Nanometer
µg	Microgram
µm	Micrometer
ccm/cm^3	Cubic centimeter
CNT	Carbon nanotubes
CPC	Condensation Particle Counter
CVD	Chemical vapor deposition
EDS	Energy-dispersive X-ray spectroscopy
dP	Particle diameter
HAADF	High-Angle Annular Dark Field
MWCNT	Multi-wall carbon nanotube
NIOSH	National Institute of Occupational Safety & Health
PM	particulate matter
SEM	Scanning Electron Microscopy
SiO	Silicon monoxide
SMPS	Scanning Mobility Particle Sizer
STEM	Scanning Transmission Electron Microcopy
SWCNT	Single-wall carbon nanotube
TEM	Transmission Electron Microscopy
UTM	Universal Testing Machine